The Astrophysical Journal, 504:1006–1019, 1998 September 10

THE EFFECT OF CURVATURE ON FLUX-ROPE MODELS OF CORONAL MASS EJECTIONS

J. Lin[1]
Yunnan Observatory, P.O. Box 110, Kunming, YN 650011, China; jun.lin@unh.edu
T. G. Forbes and P. A. Isenberg
Institute for the Study of Earth, Ocean, and Space (EOS), University of New Hampshire, Durham, NH 03824; terry.forbes@unh.edu, phil.isenberg@unh.edu
and
P. Démoulin
Département d'Astronomie Solaire et Planétaire, Observatoire de Paris, Section de Meudon, 92195 Meudon Principal Cédex, France; demoulin@mesopb.obspm.fr
Received 1997 December 10; accepted 1998 April 15

ABSTRACT

The large-scale curvature of a flux rope can help propel it outward from the Sun. Here we extend previous two-dimensional flux-rope models of coronal mass ejections to include the curvature force. To obtain analytical results, we assume axial symmetry and model the flux rope as a torus that encircles the Sun. Initially, the flux rope is suspended in the corona by a balance between magnetic tension, compression, and curvature forces, but this balance is lost if the photospheric sources of the coronal field slowly decay with time. The evolution of the system shows catastrophic behavior as occurred in previous models, but, unlike the previous models, flux ropes with large radii are more likely to erupt than ones with small radii. The maximum total magnetic energy that can be stored before equilibrium is lost is 1.53 times the energy of the potential field, and this value is less than the limiting value of 1.662 for the fully opened field. As a consequence, the loss of ideal MHD equilibrium that occurs in the model cannot completely open the magnetic field. However, the loss of equilibrium does lead to the sudden formation of a current sheet, and if rapid reconnection occurs in this sheet, then the flux rope can escape from the Sun. We also find that the field can gradually become opened without suffering any loss of equilibrium if the photospheric field strength falls below a critical value. This behavior is analogous to the opening of a spherically symmetric arcade in response to a finite amount of shear.

Subject headings: MHD — Sun: corona — Sun: flares — Sun: particle emission

1. INTRODUCTION

Models that attempt to explain the behavior of eruptive phenomena, such as solar flares, *disparitions brusques*, and coronal mass ejections (CMEs), must account for the rapid ejection of magnetic flux and plasma into the outer corona. It is often thought that the primary mechanism for driving an eruption is magnetic reconnection. However, a series of works by some of us (Forbes 1990, 1991, 1992; Forbes & Isenberg 1991; Isenberg, Forbes, & Démoulin 1993; Forbes & Priest 1995) suggest that a catastrophic loss of mechanical equilibrium, rather than reconnection, might be the primary mechanism for driving eruptions. The latter idea has long been considered by many other authors since the middle of the 1970s (e.g., Birn & Schindler 1981; Wolfson & Low 1992; Moore 1988; Low 1990, 1996), but there have been numerous mathematical difficulties in developing a model of such a catastrophic process (see Klimchuk & Sturrock 1989, for example).

The theory of catastrophes developed by Thom (1972) provides a convenient formalism for discussing such a process. This theory applies most directly to static equilibrium states characterized by a potential energy that varies in response to slow changes in the boundary conditions of the system. As these conditions vary, the system evolves quasi-statically, except at certain critical points where only a dynamic transition is possible. At a critical point the system jumps suddenly from one equilibrium state to another at a lower energy, and it is this jump that constitutes the "catastrophe."

Forbes & Isenberg (1991, hereafter Paper I) and Isenberg et al. (1993, hereafter Paper II) developed ideal MHD models with translational symmetry that are related to earlier circuit models by Van Tend & Kuperus (1978), Van Tend (1979), and Martens & Kuin (1989). The ideal models are based on a two-dimensional configuration of a flux rope nested within an arcade, and they allow for the formation of a current sheet. The frozen-flux condition at the flux-rope surface is used to determine the current flowing inside the flux rope as a function of the boundary conditions at the photosphere.

The evolution of this system takes place in two stages: the first stage stores energy, while the second releases it. During the storage phase, the evolution is assumed to be so slow (with a timescale of hours) that the evolution can be regarded as quasi-static. During the eruptive phase, mechanical equilibrium is lost, and the system evolves rapidly over an Alfvén timescale of seconds. During this phase, the flux rope jumps to a higher altitude, releasing part of the magnetic energy stored in the system.

Forbes & Isenberg (1991) found that if the flux-rope radius is larger than a particular value, a two-dimensional system with translational symmetry evolves continuously with no catastrophe. This behavior is typical of the cusp-type catastrophe, one of the seven elementary catastrophes (Poston & Stewart 1978). Forbes, Isenberg, & Priest (1994) also found that the energy

[1] Currently at EOS, University of New Hampshire, Durham, NH 03824.

released by the catastrophic loss of equilibrium is very sensitive to the choice of boundary condition. For a photospheric background field corresponding to a two-dimensional line dipole, the energy release never exceeds 1% of the stored energy, and, even worse, the radius must be extremely small, less than 10^{-3} times the scale length of the system. However, there do exist plausible boundary conditions which produce satisfactory results. In fact, it is possible to achieve energy releases as high as 21% of the stored magnetic energy and yet have the flux-rope radius as large as the scale length of the system (Forbes & Priest 1995).

Another class of storage models that has recently received much attention attempts to create an eruption by shearing the footpoints of a simply connected arcade, where all the field lines contact the boundary surface (Mikić, Barnes, & Schnack 1988; Steinolfson 1991; Inhester, Birn, & Hesse 1992; Mikić & Linker 1994; and Amari et al. 1996). Finn & Chen (1990) showed that a simply connected arcade in a two-dimensional force-free configuration with translational symmetry always remains in a stable equilibrium as the footpoints are sheared. But Inhester et al. (1992) found that the simply connected arcade can erupt once reconnection occurs. Reconnection leads to the formation of a magnetic flux rope and, therefore, a non–simply connected field.

In two-dimensional systems with axial symmetry, the eruptive behavior can be quite different. The field may become partly or even fully opened in response to a finite amount of footpoint shear (Wolfson & Low 1992; Mikić & Linker 1994), and the total energy of the system is finite rather than infinite. According to Aly (1984) and Sturrock (1991), the stored energy in any system cannot exceed the energy of the fully opened magnetic field, provided that the field lines are simply connected to the surface of the Sun. For example, they stated that the energy stored in the axial symmetric models using a Sun-centered dipole cannot exceed 1.662 times the energy of the potential field. This result has been directly checked by Mikić & Linker (1994), who found that a sheared arcade evolves toward the open configuration as its energy approaches the Aly limit. Aly's and Sturrock's analyses do not apply to configurations that have field lines that are disconnected from the Sun or that are "knotted" (i.e., not simply connected). Thus, their conclusion does not apply to the configuration we are considering in this paper.

In the present work, we modify the analyses of Papers I and II by replacing a flat solar surface and an infinitely long cylindrical flux rope with a spherical solar surface of radius R_0 and a circular flux rope of major radius (or the height from the center of the Sun) h and cross-sectional (minor) radius r_0 around the Sun, respectively. Although this model is still geometrically oversimplified compared to real CMEs, it contains two important improvements over the previous two-dimensional models. First, it includes the curvature force that is likely to be significant in driving the CMEs outward from the Sun; second, the total energy stored is now finite instead of infinite as in the previous models. As in Papers I and II, r_0 is assumed to be much smaller than the height, h, of the flux rope; that is, $r_0 \ll h$.

Although our axisymmetric model now includes curvature effects, it still has the feature that the ends of the flux rope are not anchored to the photosphere. Therefore, the possibility remains that if the ends were anchored, the catastrophic behavior we find in the present solution might be eliminated. However, there is no evidence at the present time that anchoring the ends of the flux rope prevents catastrophe behavior.

In § 2 we outline the model, and in § 3 we solve the governing equations for configuration without current sheets. In § 4 we obtain asymptotic solutions for systems with current sheets in the limit that the flux rope is far from the Sun. Finally, we summarize and discuss the physical meaning of our results in § 5.

2. DESCRIPTION OF THE MODEL

The model consists of two-dimensional equilibrium solutions in a spherical system with axial symmetry, and with $r = R_0$ being the photospheric boundary. The coronal region $r > R_0$ is assumed to be perfectly conducting, so that magnetic field lines are frozen to the plasma. A toroidal force-free magnetic flux rope is suspended in the corona at the height, h, by a balance between tension, compression, and curvature forces. The latter occurs when a straight, current-carrying flux rope is bent into a curve (Shafranov 1966). In the present work we do not address the question of how a flux rope might be formed, but several mechanisms have been suggested in previous studies (e.g., van Ballegooijen & Martens 1989; Inhester et al. 1992).

A catastrophic jump may occur before or after a neutral point (or X-point) appears, depending on the structure of the photospheric field and on the radius of the flux rope. Here we assume that the reconnection timescale is long compared to the coronal Alfvén timescale, but short compared to the timescale of the photospheric field evolution. This means that current sheets continually dissipate as they try to form during the slow evolution phase prior to eruption. However, during the eruptive phase, the system evolves so rapidly that current sheets can form because the evolution is too fast for them to dissipate.

The coronal magnetic field during the storage phase is determined by the normal field component at the photospheric boundary, and the magnetohydrostatic equations:

$$\frac{1}{c} \boldsymbol{J} \times \boldsymbol{B} = \nabla p + \boldsymbol{F}_g \,, \tag{1}$$

$$\nabla \times \boldsymbol{B} = \frac{4\pi}{c} \boldsymbol{J} \,, \tag{2}$$

$$\nabla \cdot \boldsymbol{B} = 0 \,, \tag{3}$$

where $\boldsymbol{B}$ is the magnetic field, $\boldsymbol{J}$ is the current density, p is the plasma gas pressure, $\boldsymbol{F}_g$ is gravitational force, and c is the speed of light.

By invoking the force-free approximation, we dismiss gravitational and pressure forces together in equation (1). Although these forces may be quantitatively important for some aspects of solar eruptions, they are not essential to the catastrophe behavior we consider here. This leads to

$$\boldsymbol{J} \times \boldsymbol{B} = 0 . \tag{4}$$

Solving equations (2) and (4) with the appropriate boundary condition gives the whole magnetic configuration of the system. We start by choosing a spherical coordinate system and putting its origin at the center of the Sun with the z-axis in the north direction, so equations (2) and (4) can be combined and simplified to one equation:

$$\nabla^2 A_\phi - \frac{A_\phi}{r^2 \sin^2 \theta} + \frac{1}{2r \sin \theta} \frac{d(rB_\phi \sin \theta)^2}{d(rA_\phi \sin \theta)} = 0 , \tag{5}$$

where B_ϕ is the field in azimuthal direction, and A_ϕ is the ϕ component of the vector potential $\boldsymbol{A}$ defined by

$$(B_r, B_\theta, B_\phi) = \left[\frac{1}{r \sin \theta} \frac{\partial}{\partial \theta} (\sin \theta A_\phi), \ -\frac{1}{r} \frac{\partial}{\partial r} (rA_\phi), \ \frac{1}{r} \frac{\partial}{\partial r} (rA_\theta) - \frac{1}{r} \frac{\partial A_r}{\partial \theta}\right] , \tag{6}$$

in this geometry, and A_r, A_θ, and B_ϕ all vanish outside the flux rope.

3. CONFIGURATION PRIOR TO ERUPTION

For our analysis, equation (5) can be rewritten as a Poisson equation (see Appendix A):

$$\nabla^2(A_\phi \cos \phi) = -\frac{4\pi}{c} J_\phi \cos \phi , \tag{7}$$

where J_ϕ includes the current density in the flux rope and the current sheet, if one exists. We further assume that there are no magnetic field sources at infinity, that the flux rope is located at the equatorial plane, that the flux rope is the only current source in the region $r > R_0$ prior to the eruption, and that the minor radius, r_0, of the flux rope is much smaller than its distance h from the Sun. The boundary condition at the photosphere represents a field equivalent to that produced by a point dipole at the center of the Sun. We choose a point dipole to represent the boundary field, not because we think it is the best one to use but because it allows us to compare our analysis to previous ones which have used such a boundary condition (e.g., Mikić & Linker 1994; Low & Smith 1993; Roumeliotis 1992). In fact, previous analysis of the two-dimensional systems with translational symmetry suggests that the dipole boundary condition is the least effective in producing a vigorous eruption (see Forbes et al. 1994).

The field in the region outside the flux rope can most easily be determined by representing the flux rope as a circular line current of the form

$$J_\phi(r, \theta) = \frac{I}{h} \delta(\cos \theta)\delta(r - h) , \tag{8}$$

where I is the current strength carried by the flux rope. Note that this is an approximation that is valid only outside the flux rope, since within the flux rope J_ϕ is finite and J_θ is not zero. The vector potential at the photosphere, which is just the background dipole field, is

$$A_\phi(r = R_0, \theta) = \frac{m_0 \sigma(t) \sin \theta}{R_0^2} , \tag{9}$$

where m_0 is a constant and $\sigma(t)$ is a function which slowly decreases with time. Thus, the evolution of the photospheric field corresponds to a decrease of the field such as would occur in a decaying active region, except that here our assumed symmetry makes the decay global.

Equation (7) can be solved by means of Green's method by combining it with equations (8) and (9). The solution is

$$A_\phi(r, \theta) \cos \phi = \frac{1}{c} \int_V J_\phi(r', \theta') \cos \phi' G(\boldsymbol{r}, \boldsymbol{r}') dV' - \frac{1}{4\pi} \oint_S A_\phi(R_0, \theta') \cos \phi' \left. \frac{\partial G(\boldsymbol{r}, \boldsymbol{r}')}{\partial r'} \right|_{r' = R_0} dS' , \tag{10}$$

where the volume integral is taken over the whole region with $r > R_0$ and the surface integral is taken over the surface of the Sun, namely, $r' = R_0$. The function $G(\boldsymbol{r}, \boldsymbol{r}')$ is the Green's function for our system:

$$G(\boldsymbol{r}, \boldsymbol{r}') = \frac{1}{|\boldsymbol{r} - \boldsymbol{r}'|} - \frac{R_0}{r' |\boldsymbol{r} - R_0^2 \boldsymbol{r}'/r'^2|} ,$$

which in terms of spherical coordinates can be written as

$$G(\boldsymbol{r}, \boldsymbol{r}') = \frac{1}{(r^2 + r'^2 - 2rr' \cos \gamma)^{1/2}} - \frac{1}{(r^2 r'^2/R_0^2 + R_0^2 - 2rr' \cos \gamma)^{1/2}} , \tag{11}$$

where γ is the angle between $\boldsymbol{r}$ and $\boldsymbol{r}'$ and $\cos \gamma = \cos \theta \cos \theta' + \sin \theta \sin \theta' \cos (\phi - \phi')$.

Substituting equations (8), (9), and (11) into equation (10) gives

$$A_\phi(r,\theta) = \frac{4Ih}{c\sqrt{h^2+r^2+2hr\sin\theta}}\left[\frac{(2-k^2)K(k)-2E(k)}{k^2}\right] - \frac{4IhR_0}{c\sqrt{h^2r^2+R_0^4+2hrR_0^2\sin\theta}}\left[\frac{(2-\tilde{k}^2)K(\tilde{k})-2E(\tilde{k})}{\tilde{k}^2}\right] + \frac{m_0\,\sigma(t)}{r^2}\sin\theta\,, \tag{12}$$

where K and E are complete elliptic integrals of the first and second kind, respectively, and

$$k^2 = \frac{4hr\sin\theta}{h^2+r^2+2hr\sin\theta}\,, \qquad \tilde{k}^2 = \frac{4hrR_0^2\sin\theta}{h^2r^2+R_0^4+2hrR_0^2\sin\theta}\,.$$

In a spherical coordinate system with axial symmetry, magnetic field lines are described by

$$\frac{dr}{B_r} = \frac{r\,d\theta}{B_\theta}\,,$$

which yields

$$rA_\phi \sin\theta = \text{constant}\,, \tag{13}$$

holding (with a different constant) on each field line. Figure 1 shows the magnetic field contours of our model in a meridional plane.

3.1. *Global Equilibria*

According to equation (6), the result given in equation (12) yields a magnetic field on the $\theta = \pi/2$ (equatorial) plane in terms of the series

$$B_\theta\left(r, \theta=\frac{\pi}{2}\right) = \frac{4\pi I}{ch}\sum_{n=0}^{\infty}(n+1)\left[\frac{(2n+1)!!}{(2n+2)!!}\right]^2\left[f(r,n) - \frac{h^2}{R_0 r}\left(\frac{R_0^2}{rh}\right)^{2n+2}\right] + \frac{m_0\,\sigma(t)}{r^3}\,, \tag{14}$$

where

$$f(r,n) = \begin{cases} -\dfrac{2n+2}{2n+1}\left(\dfrac{r}{h}\right)^{2n} & \text{if } r < h\,, \\ \left(\dfrac{h}{r}\right)^{2n+3} & \text{if } r > h\,. \end{cases}$$

The term containing $f(r, n)$ corresponds to the field produced by the current in the flux rope alone. By subtracting this term and setting $r = h$ in equation (14), we can deduce the external magnetic field, B_e, acting on the flux rope due to the sources

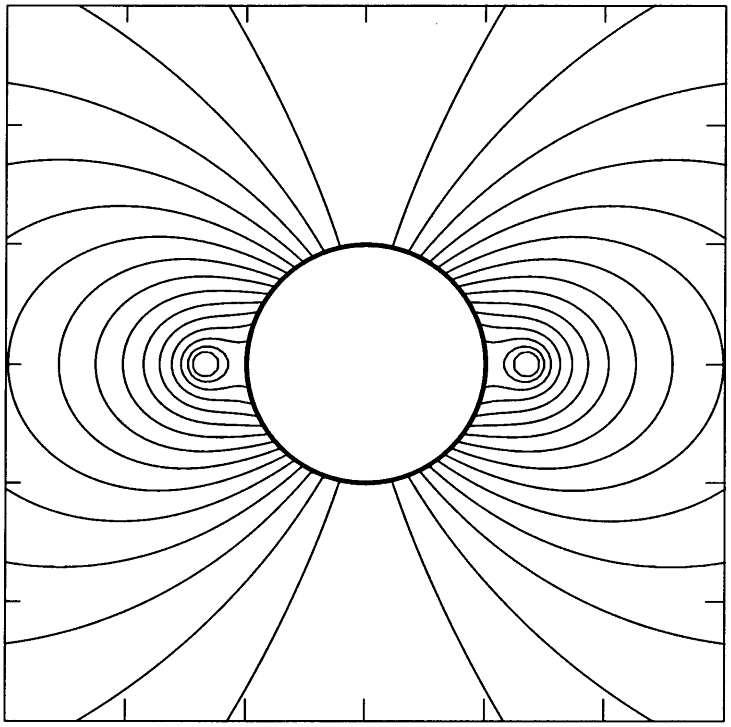

FIG. 1.—Magnetic field configuration in a meridional plane ($rA_\phi \sin\theta$ contours) when the system is at the critical point for the case of $r_{00} = 0.01$. Tick marks are spaced every solar radius in the equatorial and polar directions.

outside of it. The result is

$$B_e = -\frac{4\pi I}{cR_0}\sum_{n=0}^{\infty}(n+1)\left[\frac{(2n+1)!!}{(2n+2)!!}\right]^2 p^{2n+2} + \frac{m_0\,\sigma(t)}{h^3}$$
$$= \frac{4I}{cR_0}\left[K(p) - \frac{E(p)}{1-p^2}\right] + \frac{m_0\,\sigma(t)}{h^3}\,, \quad (15)$$

where $p = (R_0/h)^2$. Note that the external magnetic field, B_e, includes not only the contribution of the background dipole field (the third term on the right-hand side of eq. [15]) but also that of a surface current (the other terms on the right-hand side of eq. [15]), which is equivalent to an image of the flux rope beneath the surface.

In a two-dimensional system with translational symmetry, the body forces on the flux rope are all proportional to B_e, so the equilibria are situated at the positions where B_e vanishes (Papers I and II, etc.). However, this condition does not hold in the present case. The curvature of the flux rope creates an additional outward force which must be balanced by the external field, B_e. This force was calculated by Shafranov (1966), and the magnitude is equal to the current, I, times the magnetic field B_S:

$$B_S = \frac{I}{ch}\left(\ln\frac{8h}{r_0} - 1\right), \quad (16)$$

where r_0 is the minor radius of the toroidal flux rope and we have assumed that the field inside the flux rope is prescribed by Lundquist's force-free solution (see Appendix B). For a force-free flux rope, this force is always directed outward in the radial direction, and it is caused by the compression of the poloidal field along the inside edge of the torus.

Matching B_e in equation (15) and B_S in equation (16) gives the condition for global equilibrium, namely,

$$4J\left[K(p) - \frac{E(p)}{1-p^2}\right] + \frac{\sigma u}{h^3} = \frac{J}{h}\left(\ln\frac{8h}{r_0} - 1\right), \quad (17)$$

where now all lengths are normalized to R_0, the radius of the Sun, J is the current normalized to $I_0 = m_0\,c/(uR_0^2)$, and $p = 1/h^2$. The constant u is used to normalize σ to unity when J reaches unity, its maximum value.

Since the frozen-flux condition requires the magnetic field lines at the surface of the flux rope to remain unchanged, we require, according to equation (13), that

$$(h - r_0)A_R = (h - r_0)A_\phi\left(h - r_0, \frac{\pi}{2}\right) = \text{constant}\,.$$

Substituting equation (12) in this equation gives

$$hA_R = \frac{I_0}{c}\,h\left\{2J\ln\frac{8h}{r_0} - 4J + 4Jh[E(p) - K(p)] + \frac{\sigma u}{h^2}\right\} = \text{constant}\,, \quad (18)$$

to the lowest order of r_0/h. To determine h solely as a function of σ, we need to consider the local equilibrium inside the flux rope.

3.2. *Internal Equilibrium*

The distribution of current density and field inside the flux rope is arbitrary to some extent, since we are free to choose any force-free configuration initially in the same way that we are free to choose a photospheric boundary condition.

For our model, we will use Lundquist's (1950) solution, which has been extensively used in modeling coronal mass ejections (e.g., Kumar & Rust 1996). For simplicity, the calculation of the internal equilibrium is performed in a cylindrical coordinate system where B_z is along the central axis, B_ϑ is the azimuthal component, and B_ρ is the radial component relative to the axis. In this system, Lundquist's solution is

$$B_\rho = 0\,, \qquad B_\vartheta = B_0\,J_1(\lambda r)\,, \qquad B_z = B_0\,J_0(\lambda r)\,, \quad (19)$$

J_0 and J_1 are the zeroth- and first-order Bessel functions, and λ is a constant.

For a toroidal flux rope the Lundquist solution is approximately correct as long as the minor radius, r_0, is much smaller than the major radius, h (Miller & Turner 1981). Since the flux rope in our model is located in the equatorial plane, the external field B_e does not contribute to the toroidal component within the flux rope. This means that the conservation of toroidal flux simply gives

$$\Phi_t = \int_0^{2\pi}\int_0^{r_0} B_z\,\rho\,d\rho\,d\vartheta = \text{constant}\,. \quad (20)$$

Since we also have $\lambda B_z = 4\pi j_z/c$ (the force-free condition), equation (20) reduces to

$$\Phi_t = \frac{4\pi}{\lambda c}\int_0^{2\pi}\int_0^{r_0} j_z\,\rho\,d\rho\,d\vartheta = \frac{4\pi I}{\lambda c}\,,$$

with

$$\frac{I}{\lambda} = \text{constant} , \tag{21}$$

where I is the total current in the flux rope.

At the surface of the flux rope, B_z is equal to zero so $J_0(\lambda r_0) = 0$ there. Hence, λr_0 is the first zero of J_0, namely, $\lambda r_0 = 2.405$. Substituting this in equation (21), we find

$$r_0 I = \text{constant} , \tag{22}$$

which determines the relationship between the flux-rope radius r_0 and the current I.

3.3. *Evolution of the System*

Equations (17) and (18) indicate that equilibria can only exist for flux-rope currents less than a particular value. This can be seen by using equation (17) to eliminate σu in equation (18), differentiating the result with respect to h, and setting $dJ/dh = 0$ with

$$r_0 = \frac{r_{00} I_0}{I} = \frac{r_{00}}{J} , \tag{23}$$

where I_0 and J are defined as before. At the current maximum the flux-rope equilibrium height h_0 is related to r_{00} by

$$3 \ln \frac{8h_0}{r_{00}} - 2 + 8h_0 \left[\frac{2 - 4p_0^2}{(1 - p_0^2)^2} E(p_0) + \frac{3p_0^2 - 2}{1 - p_0^2} K(p_0) \right] = 0 , \tag{24}$$

where $p_0 = 1/h_0^2$. We will refer to this state, $h = h_0$, as the *maximum current point*, and r_{00} corresponds to the radius of the flux rope at this point. When r_{00} vanishes, h_0 goes to unity.

At the maximum current point, we set the constant on the right-hand side of equation (18) equal to $h_0 A_R^0 I_0/c$ and use equation (17) to eliminate σu in equation (18), giving

$$\begin{aligned} hA_R &= h_0 A_R^0 \frac{I_0}{c} \\ &= h_0 \frac{I_0}{c} \left\{ 3 \ln \frac{8h_0}{r_{00}} - 5 + 4h_0 \left[\frac{2 - p_0^2}{1 - p_0^2} E(p_0) - 2K(p_0) \right] \right\} . \end{aligned}$$

Thus

$$A_R^0 = 3 \ln \frac{8h_0}{r_{00}} - 5 + 4h_0 \left[\frac{2 - p_0^2}{1 - p_0^2} E(p_0) - 2K(p_0) \right] ; \tag{25}$$

with this explicit expression for the constant in equation (18), we have

$$J = \frac{A_R^0 h_0}{h} \left\{ 3 \ln \frac{8h}{r_0} - 5 + 4h \left[\frac{2 - p^2}{1 - p^2} E(p) - 2K(p) \right] \right\}^{-1} . \tag{26}$$

Returning to equation (17) at the maximum current point, we obtain

$$u = h_0^2 \left(\ln \frac{8h_0}{r_{00}} - 1 \right) + 4h_0^3 \left[\frac{E(p_0)}{1 - p_0} - K(p_0) \right] . \tag{27}$$

The current J is determined self-consistently from the frozen-flux condition (18), which depends on r_{00}, the radius of the flux rope at the maximum current point. As mentioned before, σ is unchanged during an eruption (or catastrophe), therefore the h-σ curve reveals where a catastrophic loss of equilibrium can occur. Substituting equation (26) in equation (17) to eliminate J leads to

$$\sigma = \frac{hh_0 A_R^0}{u} \frac{\ln(8h/r_0) - 1 + 4h[E(p)/(1 - p^2) - K(p)]}{3 \ln(8h/r_0) - 5 + 4h\{[(2 - p^2)/(1 - p^2)]E(p) - 2K(p)\}} , \tag{28}$$

which describes the flux-rope equilibrium height h as a function of the photospheric boundary condition parameter σ.

The dependence of h as a function of σ is illustrated in Figure 2 for $r_{00} = 10^{-2}$. The equilibrium curve in Figure 2 exhibits the switchback shape characteristic of a catastrophic system. To model a CME, we suppose that the flux rope starts somewhere on the portion of the curve which is close to the solar surface, for example, at $\sigma = 1$, $h = 1.186$. At this location the flux rope is stable to displacements in any direction (Forbes 1990, 1991), but if the photospheric field slowly weakens with time (corresponding to decreasing σ), a stable equilibrium will eventually become impossible. As σ decreases, the flux rope moves leftward and upward along the equilibrium curve until it reaches the lower nose point at $\sigma = 0.9458$, $h = 1.340$. Once this critical point is reached, the forces pushing the flux rope away from the Sun can no longer be balanced by the magnetic

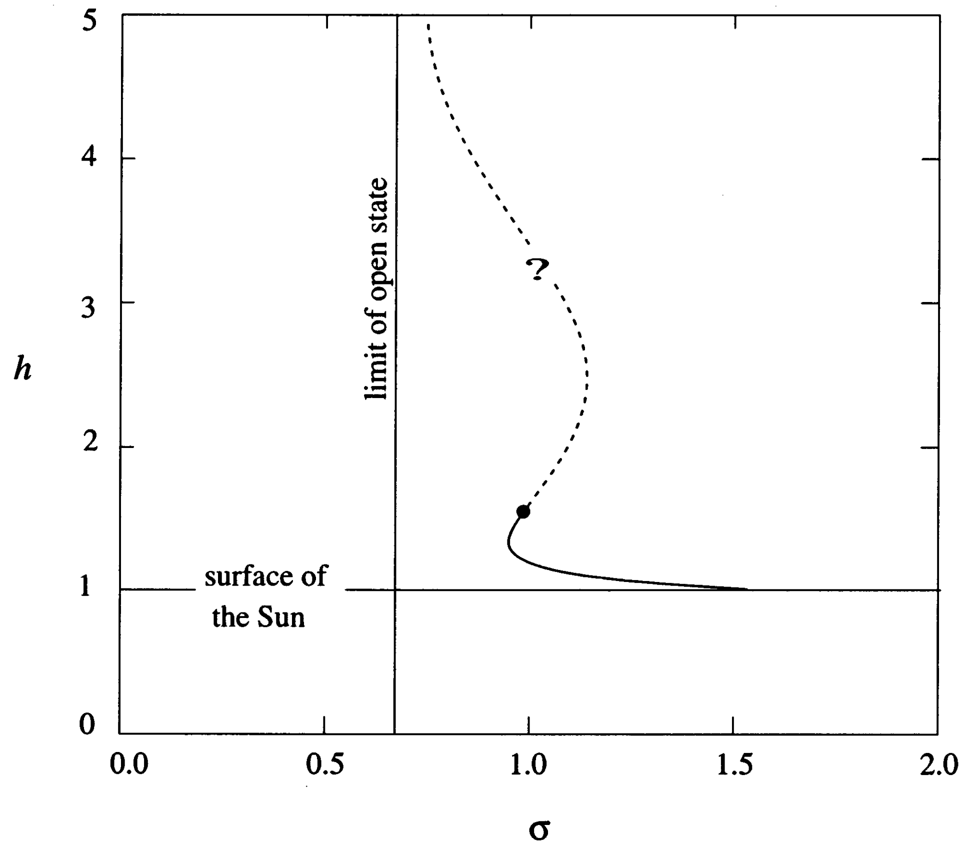

FIG. 2.—Equilibrium height h as a function of dipole strength σ for $r_{00} = 0.01$. At $\sigma = 0.741$, $h = \infty$, and the field has reached the open limit. The solid circle indicates the position of current sheet formation, and the dashed line is a hypothetical curve for ideal MHD equilibria containing current sheets.

tension which holds the flux rope down. Thus, at the critical point (i.e., the nose point), the flux rope loses equilibrium and is ejected outward, away from the Sun. As the flux rope moves outward, the horizontal field at the equator decreases until an X-type neutral line appears. In the ideal MHD limit, the field around the neutral line immediately collapses to a current sheet that grows in length as the flux rope moves farther from the Sun. However, as we will show in the next section, the increasing magnetic tension associated with the growth of the sheet eventually stops the outward movement of the flux rope and leads to the formation of a new equilibrium configuration without opening the field.

Because of the mathematical difficulty of solving the Poisson's equation (7) for a mixed boundary condition (i.e., the solar surface plus current sheet), we are not able to determine a general analytical solution that includes a current sheet of arbitrary size. Thus, we can only be sure that an eruption occurs when the critical point h_c appears before the formation of a current sheet. The location of the critical point is determined by setting $d\sigma/dh = 0$ in equation (28), while the location where a current sheet forms is determined by setting $B_\theta(r = R_0 = 1, \pi/2) = 0$ in equation (14) in conjunction with the equilibrium condition (28). We label this location as $\sigma_s(h_s)$, and it is given by

$$\sigma_s = \frac{A_R^0 h_0}{u} \left\{ \frac{\ln(8Jh_s/r_{00}) + 2h_s[E(p_s) - K(p_s)] - 2}{2[E(1/h_s)(1 + p_s)/(1 - p_s) - K(1/h_s)]} + \frac{1}{h_s} \right\}^{-1} , \tag{29}$$

where $p_s = 1/h_s^2$. Figure 3 plots the variations of $(h_c - h_s)$ versus r_{00}, from which we see that for sufficiently small r_{00}, a current sheet forms before catastrophe occurs. The radius at which this occurs is $r_{00} \approx 2 \times 10^{-3}$.

Figure 1 shows field lines ($rA_\phi \sin\theta$ contours) for the equilibrium configuration at the critical point for the case of $r_{00} = 0.01$. Although h_c is less than h_{ne} in this case, the fractional difference $(h_s - h_c)/h_c$ is only 1.1%. This is reflected in Figure 1 by the fact that the X-point lies just below the photosphere at $\theta = \pi/2$.

3.4. *Energetics*

One of the important aspects of the model is to evaluate the free magnetic energy stored in the system before catastrophe occurs. The stored magnetic energy of the system before catastrophe is equal to the work required to move the flux rope from infinity to the critical point. Thus, the energy is given by

$$W = -\int_P F(h, \Phi)dh + \frac{1}{c}\int_P I(h, \Phi)d\Phi , \tag{30}$$

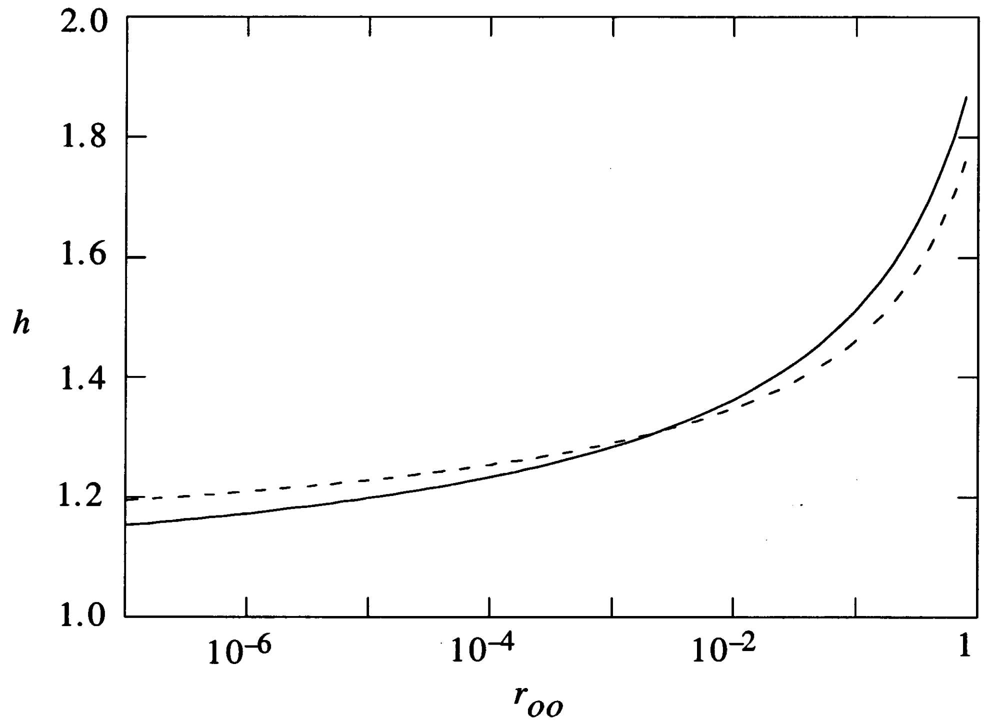

FIG. 3.—Comparisons of two types of equilibrium heights, namely, the critical-point height (the equilibrium height of the flux rope when it is at the critical point (*dashed curve*), and the current sheet formation height (the equilibrium height of the flux rope when an X-line appears at surface of the Sun (*solid curve*). The two heights are shown as functions of flux-rope radius r_{00}, and are equal to each other at around $r_{00} = 2.5 \times 10^{-3}$.

where the force $F(h, \Phi)$ is

$$F(h, \Phi) = 2\pi h \frac{I}{c}(B_S - B_e)$$

$$= 2\pi\left(\frac{I_0}{c}\right)^2 J\left\{4Jh\left[K(p) - \frac{E(p)}{1-p^2}\right] + \frac{\sigma u}{h^2} - J\left(\ln\frac{8Jh}{r_{00}} - 1\right)\right\}, \tag{31}$$

the flux rope current $I = I_0 J$ is given by equation (26), the magnetic flux Φ between the flux rope surface and the photosphere is

$$\Phi = hA_R - R_0 A_0 \tag{32}$$

with $A_0 = A_\phi(R_0, \pi/2)$, and P is a path of integration in the h-σ plane from infinity, where $J = 0$, to the critical point. The work done in evolving from one state to another is independent of the path P taken between the two states. For simplicity, we choose P such that $d\Phi = 0$, and then the second integral in equation (30) vanishes.

Thus, we calculate the energy of the configuration at height h by computing the work required to move the flux rope from infinity to h. This process need not be ideal, so we can assume that reconnection at any X-line is so rapid that no current sheet forms (see Paper II). The energy W of any state without a current sheet is then given by equations (30) and (31) with σ held constant. Therefore, defining W^* as the energy at the critical point, we find that the free energy stored in the system prior to eruption is

$$W^* = 2\pi\left(\frac{I_0}{c}\right)^2 J_c^2 h_c\left\{2h_c[E(p_c) - K(p_c)] + \left(\ln\frac{8J_c h_c}{r_{00}} - \frac{3}{2}\right)\right\} - \pi\left(\frac{I_0}{c}\right)^2 \int_{h_c}^{\infty} J^2\, dh\,, \tag{33}$$

where J_c is J at the critical point, and $p_c = 1/h_c^2$.

To facilitate comparison with previous studies, we also calculate the total magnetic energy of the system, which is defined as $W_{\rm total} = W_{\rm potential} + W$, where $W_{\rm potential}$ is just the potential energy associated with the photospheric field sources. At the critical point,

$$W^*_{\rm potential} = \frac{1}{3}\left(\frac{I_0}{c}\right)^2 (\sigma_c u)^2\,, \tag{34}$$

where σ_c is σ at this point. Figure 4 plots $W^*_{\rm total}/W^*_{\rm potential}$ against r_{00}, the flux-rope radius at the point of maximum current on the equilibrium curve. The figure shows that although $W^*_{\rm total}/W^*_{\rm potential}$ increases with r_{00}, it remains less than 1.662, the ratio for a fully opened field (Aly 1984; Sturrock 1991; Low & Smith 1993).

The solid curve in Figure 4 corresponds to configurations of the system at critical points without an X-line, and when these configurations erupt, they generate current sheets which are attached to the solar surface. By contrast, the dashed curve

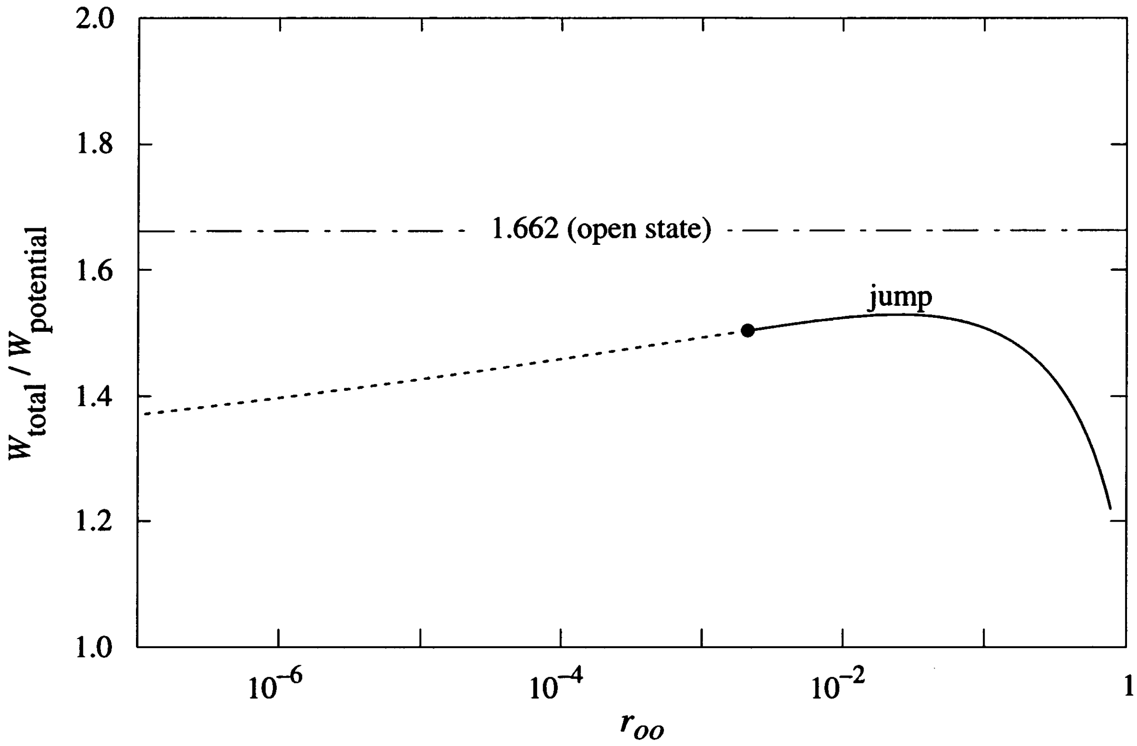

FIG. 4.—Ratio of total magnetic energy to potential magnetic energy at the critical point as a function of the flux-rope radius r_{00}. It is not known whether there are any catastrophes for $r_{00} < 2.5 \times 10^{-3}$ (*dashed portion of curve*), because the stability of the equilibria in this region has not been determined. Note that the stored energy is always less than that of the fully opened field (*horizontal dash-dotted line*).

corresponds to the configurations containing an X-line prior to eruption. Such configurations occur if r_{00} is less than 2.5×10^{-3}, and if we assume that the coronal reconnection timescale is much smaller than the timescale for the evolution of the photospheric field. Thus, unlike the situation during the eruption of the flux rope, the appearance of an X-line during the slow evolution along the equilibrium curve does not lead to the formation of a large-scale current sheet. (Analyses of reconnection rate in flares by Poletto & Kopp 1986 and Lin et al. 1995 and X-ray bright points by Parnell, Priest, & Titov (1994) indicate that the coronal reconnection timescale is longer than the Alfvén timescale but shorter than the convective timescale for the evolution of the photospheric field.)

When a configuration containing an X-line erupts, a current sheet immediately appears. Consequently, in the absence of any practical method for solving our equations when a current sheet of finite length is present, we cannot analyze the ideal MHD stability of the configurations lying on the dashed curve in Figure 4. Although we know equilibria exist at these locations, we do not know whether an upward vertical displacement will create an inward restoring force or an outward driving force.

Further, we notice that in the present model, because of the curvature of the flux rope, systems with flux ropes of small radius have less energy than those with flux ropes of large radius—behavior which is opposite to that in the previous models with translational symmetry. This difference is due to the fact that the curvature force becomes infinitely large as the radius, r_0, tends to zero. Therefore, to have equilibrium as r_0 tends to zero, the current J in the flux rope must also tend to zero. However, as the current goes to zero, so does the free magnetic energy, and thus the net effect of the curvature force at small radii is to reduce the amount of free energy stored in the system.

4. ASYMPTOTIC BEHAVIOR OF THE SYSTEM

If a current sheet of an arbitrary size exists, the boundary-value problem for the Poisson equation (7) becomes much more difficult. At the surface of the sphere, the boundary condition is still

$$A_\phi(R_0, \theta, \phi) = \frac{m_0 \sigma(t) \sin \theta}{R_0^2}, \tag{35}$$

but on the current sheet

$$rA_\phi(r, \pi/2, \phi) = R_0 A_0, \qquad R_0 \le r \le q, \tag{36}$$

where $A_0 = m_0 \sigma / R_0^2 = I_0 \sigma u / c$.

Because of the additional complexity introduced by disk geometry of the current sheet, we can no longer obtain an analytical solution, although a numerical solution is possible, at least, in principle (Tur & Priest 1985). However, we can investigate the asymptotic behavior of the system when the current sheet becomes very large. This case occurs when the flux rope is far from the Sun, and the length, q, of the current sheet, is much larger than R_0. In this limit the Sun can be regarded as a point, and the boundary condition in equation (35) can be ignored, since at large distance the dipole contribution becomes negligible compared to that of the current sheet. The boundary-value problem now consists of equation (7) with J_ϕ given in equation (8) and the boundary condition on the disk of current prescribed by equation (36). The solution is

$$A_\phi = -\frac{\pi I h}{c}\sum_{n=0}^{\infty}\frac{(-1)^n(2n-1)!!}{2^n(n+1)!}\frac{r_<^{2n+1}}{r_>^{2n+2}}P_{2n+1}^1(\cos\theta) + \sum_{n=0}^{\infty}A_{2n+1}P_{2n+1}^1(\xi)Q_{2n+1}^1(i\zeta)\,, \tag{37}$$

where P and Q are Legendre functions of the first and second kinds, $r_< = \min(h, r)$, and $r_> = \max(h, r)$. The variables ζ and ξ are the *oblate spheroidal coordinates*, which are related to (x, y, z) and (r, θ, ϕ) as

$$\begin{aligned} x &= r\sin\theta\cos\phi = q\sqrt{(1+\zeta^2)(1-\xi^2)}\cos\phi\,,\\ y &= r\sin\theta\sin\phi = q\sqrt{(1+\zeta^2)(1-\xi^2)}\sin\phi\,,\\ z &= r\cos\theta = q\zeta\xi\,, \end{aligned} \tag{38}$$

with $0 \le \zeta < \infty$ and $|\xi| \le 1$. Here q is the radius of the disk (or current sheet) and

$$A_{2n+1} = (-1)^n\frac{4n+3}{(n+1)(2n+1)}\left[-\frac{A_0R_0}{\pi q}\frac{(2n)!!}{(2n+1)!!} + \frac{2I}{c}(1+\zeta_0^2)^{1/2}\frac{(2n-1)!!}{(2n+2)!!}Q_{2n+1}^1(i\zeta_0)\right], \tag{39}$$

with $\zeta_0 = [(h/g)^2 - 1]^{1/2}$. Consequently, the magnetic field configuration is given by $r\sin\theta A_\phi =$ constant, as shown in Figure 5, which corresponds to the limit of the open state of the system. By taking the curl of expression (37) and evaluating at $\theta = \pi/2$, we obtain the field in the equatorial plane, namely,

$$\begin{aligned} B_r &= 0\,,\\ B_\phi &= 0\,,\\ B_\theta &= f_0(r) + \frac{2}{q\zeta}\left\{\frac{A_0R_0}{\pi q}\frac{1}{1+\zeta^2} + \frac{I}{c}\sqrt{1+\zeta_0^2}\sum_{k=0}^{\infty}\frac{4k+3}{(k+1)(2k+1)}\left[\frac{(2k+1)!!}{(2k)!!}\right]^2 Q_{2k+1}^1(i\zeta_0)Q_{2k+1}(i\zeta)\right\} \end{aligned} \tag{40}$$

for $r \ge q$, where

$$f_0(r) = \frac{4I}{ch}\begin{cases} -E\left(\frac{r}{h}\right)\Big/\left[1-\left(\frac{r}{h}\right)^2\right] & \text{if } r < h\,,\\ \frac{h}{r}\left\{E\left(\frac{h}{r}\right)\Big/\left[1-\left(\frac{h}{r}\right)^2\right] - K\left(\frac{h}{r}\right)\right\} & \text{if } r > h\,, \end{cases}$$

and $\zeta = [(r/q)^2 - 1]^{1/2}$. Note that the magnetic field goes to infinity at the tip of the current sheet, $r = q$ or $\zeta = 0$ in equation (40), unless the following condition is satisfied:

$$\begin{aligned} \frac{A_0R_0}{\pi q} &= \frac{I}{c}\sqrt{1+\zeta_0^2}\sum_{k=0}^{\infty}\frac{(-1)^k(4k+3)}{(k+1)(2k+1)}\frac{(2k+1)!!}{(2k)!!}Q_{2k+1}^1(i\zeta_0)\\ &= \frac{I}{c}\frac{2s}{\sqrt{1-s^2}}\,, \end{aligned} \tag{41}$$

where s is defined as q/h. This condition forces B_θ to vanish at the tip of the current sheet and form a Y-point there as shown in Figure 5, in order to keep the whole current sheet in a force-free state.

Also note that the first term on the right-hand side of equation (37) or equation (40) is due to the flux rope alone, and that subtracting this term simply gives the external field B_e:

$$\begin{aligned} B_e &= \frac{2I}{ch\zeta_0}\left\{\frac{2s^2}{\sqrt{1-s^2}} + (1+\zeta_0^2)\sum_{k=0}^{\infty}\frac{4k+3}{(k+1)(2k+1)}\left[\frac{(2k+1)!!}{(2k)!!}\right]^2 Q_{2k+1}^1(i\zeta_0)Q_{2k+1}(i\zeta_0)\right\}\\ &= \frac{I}{ch}\left(\frac{2s^3}{1-s^2} - 2s + \ln\frac{1+s}{1-s}\right), \end{aligned}$$

where equation (41) has been used. The balance between B_e and B_S given by equation (16) yields the global equilibrium, and the relation of r_0 to J in equation (23) still applies, since as h tends to infinity, r_0/h goes to a constant which is much smaller than unity. This constant is around 0.007 for the case of $r_{00} = 0.01$. Thus, we have

$$\frac{2s^3}{1-s^2} - 2s + \ln\frac{1+s}{1-s} = \ln\frac{8Jh}{r_{00}} - 1\,. \tag{42}$$

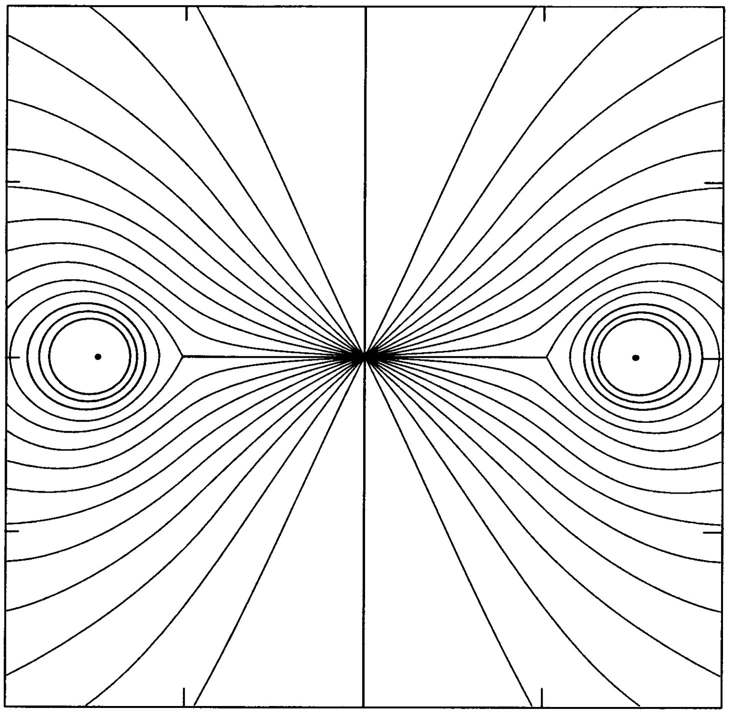

FIG. 5.—Asymptotic magnetic field configuration in a meridional plane ($rA_\phi \sin\theta$ contours) when the current sheet length is much larger than a solar radius. The case shown is for $r_{00} = 0.01$, and field lines near the axis of the flux rope (indicated by dots) are not drawn. Tick marks are spaced every disk radius in the equatorial and polar directions.

Then, using the frozen-flux condition at the surface of the flux rope leads to

$$h_0 A_R^0 \frac{I_0}{c} = hA_R$$

$$= 2h\left[\frac{I}{c}\ln\frac{8Jh}{r_{00}} + \frac{A_0 R_0}{\pi q} s \tan^{-1}\left(\frac{s}{\sqrt{1-s^2}}\right) - \frac{I}{c}\left(\ln\frac{1+s}{1-s} - 2s\right)\right], \tag{43}$$

where both the constants h_0 and A_R^0 are the same as before. Using equations (41) and (42) to eliminate $A_0 R_0/\pi q$ and the logarithmic term in equation (43), respectively, gives

$$A_R^0 h_0 = 2Jh\left[1 + \frac{2s^3}{1-s^2} + \frac{2s^2}{\sqrt{1-s^2}} \tan^{-1}\left(\frac{s}{\sqrt{1-s^2}}\right)\right]. \tag{44}$$

Substituting equation (44) and $A_0 = I_0 \sigma u/c$ into equation (41), we find

$$\sigma = \frac{\pi s^2 A_R^0 h_0}{u\sqrt{1-s^2}}\left[1 + \frac{2s^3}{1-s^2} + \frac{2s^2}{\sqrt{1-s^2}} \tan^{-1}\left(\frac{s}{\sqrt{1-s^2}}\right)\right]^{-1}. \tag{45}$$

Equations (42) and (44) determine s and Jh uniquely for a given r_{00}, reducing s and Jh to constants. Thus, according to equation (45), σ is also a constant. Plotting h against σ gives the vertical line in Figure 2, which is the limit of the open field state at $\sigma = 0.741$ and $r_{00} = 0.01$. Therefore, an open field configuration can be reached by reducing the attractive force of the Sun's dipole field below a certain value, although no loss of equilibrium is involved in such a transition. This behavior is analogous to that found by Mikić & Linker (1994) for the opening of an arcade system when the shear at the footpoints exceeds a particular value. Due to the lack of a general solution for the configuration with a current sheet of arbitrary size, the complete h-σ relation remains unknown (The dashed curve in Fig. 2 is a hypothetical solution.)

For any value of σ greater than the value giving an open field, the force at infinity in the asymptotic solution is always downward. This means that a loss of equilibrium can never create an open field, and this result holds true for any photospheric boundary condition, since the asymptotic solution is independent of the form of the photospheric field.

5. CONCLUSIONS

Our investigation shows that the effect of large-scale curvature in flux-rope models of coronal mass ejections is to reverse the relation between the radius of the flux rope and the total amount of stored magnetic energy. In the previous two-dimensional models with infinitely long, straight flux ropes, the energy decreases with increasing radius. However, for the finite-length, curved flux rope discussed in this paper, the stored energy at first increases but then decreases. This change in behavior is caused by the fact that the curvature force becomes infinite as the radius tends to zero, and equilibrium cannot be sustained unless the flux-rope current is reduced as the radius decreases. The result of reducing the current is to lower the magnetic energy stored in the configuration.

The change in the functional behavior with radius has important consequences for the conditions required to trigger an eruption. In both straight and curved flux-rope models, eruption does not occur unless the stored energy exceeds a threshold value. Although we are not able to determine the exact value of the threshold energy for the curved flux-rope case, we are able to show that it is less than 1.51 times the coronal potential energy and that eruption still occurs for any radius greater than 2.5×10^{-3} solar radii. Therefore, when curvature is important, configurations with large flux ropes are more likely to produce an energetic eruption than configurations with small ones.

For the specific case of a Sun-centered dipole, the ratio of the total magnetic energy to the potential magnetic energy ($W_{\rm total}/W_{\rm potential}$) never exceeds 1.53. Since this value is less than the ratio 1.662 for the open field, a loss of equilibrium cannot fully open the field to infinity. This result suggests that even the models which have some field lines disconnected from the boundary may still be subject to the restrictions discussed by Aly (1991) and Sturrock (1991). The main consequence of a loss of equilibrium is that it creates a current sheet where rapid reconnection can take place. With rapid reconnection it is possible for the flux rope to escape to infinity and for all of the magnetic energy stored in the corona to be released.

In addition to the specific case of a Sun-centered dipole, we have also analyzed equilibria with a current sheet in the limit that the flux rope is far from the Sun. This asymptotic analysis, which is valid for quite general boundary conditions, shows explicitly that at large distance the attractive force of the current sheet grows more rapidly than the repulsive force caused by the curvature of the flux rope. Thus, for any boundary conditions with our geometry, a loss of equilibrium never causes the field to become fully opened. However, as the strength of the normal field at the boundary decreases, the configuration approaches the open state without ever experiencing a loss of equilibrium, and small changes in the photospheric field strength produce large changes in the equilibrium height (see Fig. 2). This behavior suggests that even if no loss of ideal MHD equilibrium occurs, some type of eruptive behavior involving reconnection is likely as the photospheric field weakens.

Several important issues still remain to be investigated before the usefulness of the flux-rope models can be satisfactorily determined. First of all, there is the unknown effect of anchoring the ends of the flux rope in the photosphere. Although anchoring the ends might make an eruption more difficult, it is not clear that it would prevent a loss of equilibrium from occurring. Second, there is the question of how the two-dimensional equilibria will be affected by the kink instability. Such instabilities are inherently three-dimensional and will always occur, even when all the field lines are anchored to the solar surface, if the flux rope is sufficiently twisted (Hood 1990). Finally, there should be a smooth continuum of solutions between flux-rope and arcade models, since an arcade is equivalent to a flux rope with its toroidal axis below the surface of the Sun. Current observations suggest that if flux ropes do exist prior to eruption of CMEs, they are nested with an extensive arcade system from which they are not easily distinguished (Koutchmy 1997). All of these issues will be difficult to resolve unless progress can be made in developing three-dimensional models.

J. L. gratefully acknowledges the K. C. Wong Education Foundation, Hong Kong, which supported his visit to the University of New Hampshire during 1996. He also wishes to thank T. G. F., P. A. I., and the other members of the Solar-Terrestrial Theory Group at UNH for their hospitality during his visit there. The work of T. G. F. was supported by NASA grants NAGW-4856 and NAG 5-1479, and partly by the Observatoire de Meudon, France. The work of P. A. I. was supported by NASA grant NAG 5-1479.

APPENDIX A

DERIVATION OF POISSON'S EQUATION FOR A_ϕ

To derive equation (7) for the vector potential component A_ϕ, we start with Ampère's law:

$$\nabla \times \boldsymbol{B} = \frac{4\pi}{c} \boldsymbol{J} , \tag{A1}$$

and substitute $\boldsymbol{B} = \nabla \times \boldsymbol{A}$, which leads to

$$\nabla \times (\nabla \times \boldsymbol{A}) = -\nabla^2 \boldsymbol{A} = \frac{4\pi}{c} \boldsymbol{J} ,$$

upon applying the Coulomb gauge $\nabla \cdot \boldsymbol{A} = 0$. Thus, for the ϕ component, we have

$$[\nabla^2 \boldsymbol{A}]_\phi = -\frac{4\pi}{c} J_\phi . \tag{A2}$$

Since the unit vectors in spherical coordinates are functions of position, the left-hand side of equation (A2) is

$$[\nabla^2 \boldsymbol{A}]_\phi = \nabla^2 A_\phi - \frac{A_\phi}{r^2 \sin^2 \theta} \tag{A3}$$

(see Morse & Feshbach 1953, p. 116). Substituting equation (A3) in equation (A2) yields

$$\nabla^2 A_\phi - \frac{A_\phi}{r^2 \sin^2 \theta} = -\frac{4\pi}{c} J_\phi ,$$

which is equivalent to

$$\nabla^2(A_\phi \cos \phi) = -\frac{4\pi}{c} J_\phi \cos \phi , \tag{A4}$$

which is equation (7).

APPENDIX B

DETERMINATION OF THE SHAPE FACTOR IN SHAFRANOV'S EQUATION

Shafranov's expression for the external magnetic field, B_S, needed to maintain equilibrium in a thin, force-free flux rope, is

$$B_S = \frac{I}{ch}\left(\ln\frac{8h}{r_0} - \frac{3}{2} + \frac{l_i}{2}\right) , \tag{B1}$$

where l_i is the internal self-inductance per unit length of the flux rope. This inductance, which is associated with the toroidal current density j_z (in the coordinate system described in § 3.2), depends on the shape of the current density distribution inside the flux rope. In most applications the current density is assumed to be uniform inside the flux rope, which gives $l_i = \frac{1}{2}$. However, in our case, the current density is prescribed by the Lundquist (1950) solution (eq. [19]), for which

$$j_z = \frac{c}{4\pi} \lambda B_0 J_0(\lambda r) . \tag{B2}$$

According to Shafranov (1966), the general formula for l_i is

$$l_i = \frac{c^2 W_z}{\pi h I^2} , \tag{B3}$$

where

$$I = 2\pi \int_0^{r_0} j_z r \, dr \tag{B4}$$

and

$$W_z = \frac{1}{8\pi} \int_V B_z^2 \, dV ; \tag{B5}$$

here the volume integral in equation (B5) is taken over the whole volume of the flux rope. Substituting equation (B2) in equations (B4) and equation (19) in equation (B5) yields

$$l_i = 1 , \tag{B6}$$

so equation (B1) becomes

$$B_S = \frac{I}{ch}\left(\ln\frac{8h}{r_0} - 1\right) . \tag{B7}$$

REFERENCES

Aly, J. J. 1984, ApJ, 283, 349
———. 1991, ApJ, 375, L61
Amari, T., Lucianai, J. F., Aly, J. J., & Tagger, M. 1996, A&A, 306, 913
Birn, J., & Schindler, K. 1981, in Solar Flare Magnetohydrodynamics, ed. E. R. Priest (New York, London, Paris: Gordon & Breach), 337
Finn, J. M., & Chen, J. 1990, ApJ, 349, 345
Forbes, T. G. 1990, J. Geophys. Res., 95, 11919
———. 1991, Geophys. Astrophys. Fluid Dyn., 62, 15
———. 1992, in IAU Colloq. 133, Eruptive Solar Flares, ed. Z. Švestka, B. V. Jackson, & M. E. Machado (New York: Springer), 79
Forbes, T. G., & Isenberg, P. A. 1991, ApJ, 373, 294 (Paper I)
Forbes, T. G., Isenberg, P. A., & Priest, E. R. 1994, Sol. Phys., 150, 245
Forbes, T. G., & Priest, E. R. 1995, ApJ, 446, 377
Hood, A. W. 1990, Comput. Phys. Rep., 12, 177
Inhester, B., Birn, J., & Hesse, M. 1992, Sol. Phys., 138, 257
Isenberg, P. A., Forbes, T. G., & Démoulin, P. 1993, ApJ, 417, 368 (Paper II)
Klimchuk, J. A., & Sturrock, P. A. 1989, ApJ, 345, 1034
Koutchmy, S. 1997, in Theoretical and Observational Problems Related to Solar Eclipses, ed. Z. Mouradian & M. Stavinschi (Dordrecht: Kluwer), 39
Kumar, A., & Rust, D. M. 1996, J. Geophys. Res., 101(A7), 15667
Lin, J., Forbes, T. G., Priest, E. R., & Bungey, T. N. 1995, Sol. Phys., 159, 275
Low, B. C. 1990, ARA&A, 28, 205
———. 1996, Sol. Phys., 167, 217
Low, B. C., & Smith, D. F. 1993, ApJ, 410, 412
Lundquist, S. 1950, Ark. Fys., 2, 361
Martens, P. C. H., & Kuin, N. P. M. 1989, Sol. Phys., 122, 263
Mikić, Z., Barnes, D. C., & Schnack, D. D. 1988, ApJ, 328, 830

Mikić, Z., & Linker, J. A. 1994, ApJ, 430, 898
Miller, G., & Turner, L. 1981, Phys. Fluids, 24(2), 363
Moore, R. L. 1988, in Max 1991: Flare Research at the Next Solar Maximum, Workshop 1, Science Objectives, ed. R. C. Canfield & B. R. Dennis (NASA TM-101259; Washington, DC: NASA Goddard Space Flight Center), 97
Morse, P. M., & Feshbach, H. 1953, Methods of Theoretical Physics (New York: McGraw-Hill)
Parnell, C. E., Priest, E. R., & Titov, V. S. 1994, Sol. Phys., 153, 217
Poletto, C. E., & Kopp, R. A. 1986, in The Lower Atmosphere of Solar Flares, ed. D. F. Neidig (Sunspot: NSO), 453
Poston, T., & Stewart, I. 1978, Catastrophe Theory and Its Applications (San Francisco: Pitman)
Roumeliotis, G. 1992, BAAS, 24, 776
Shafranov, V. D. 1966, Rev. Plasma Phys., 2, 103
Steinolfson, R. S. 1991, ApJ, 382, 677
Sturrock, P. A. 1991, ApJ, 380, 655
Thom, R. 1972, Stabilité structurelle et morphogénèse (New York: Benjamin)
Tur, T. J., & Priest, E. R. 1985, Rep. Prog. Phys., 48, 955
van Ballegooijen, A. A., & Martens, P. C. H. 1989, ApJ, 343, 971
Van Tend, W. 1979, Sol. Phys., 61, 89
Van Tend, W., & Kuperus, M. 1978, Sol. Phys., 59, 115
Wolfson, R., & Low, B. C. 1992, ApJ, 391, 353